

Alexandra Ros
Wibke Hellmich
Jan Regtmeier
Thanh Tu Duong
Dario Anselmetti

Experimental Biophysics
and Applied Nanosciences,
Physics Department,
Bielefeld University,
Bielefeld, Germany

Received December 15, 2005
Revised February 24, 2006
Accepted February 27, 2006

Research Article

Bioanalysis in structured microfluidic systems

Microfluidic and lab-on-a-chip devices have attracted widespread interest in separation sciences and bioanalysis. Recent designs in microfluidic devices extend common separation concepts by exploiting new phenomena for molecular dynamics on a length scale of 10 μm and below, giving rise to novel manipulation tools and nonintuitive phenomena for microseparations. Here, we focus on three very recent developments for bioseparations based on tailored microfluidic systems: Single cell navigation, trapping and steering with subsequent on-chip lysis, protein separation and LIF detection (Section 3.1), then we report dielectrophoretic trapping and separation of large DNA fragments in structured microfluidic devices (Section 3.2). Finally, a paradoxical migration phenomenon based on thermal fluctuations, periodically arranged microchannels and a biased alternating current electric field is presented in Section 3.3.

Keywords: DNA / Microfluidic device / Migration phenomena / Protein / Single cell analytics
DOI 10.1002/elps.200500923

1 Introduction

Microfluidic separation and analysis of biological compounds represent an ever growing discipline in separation sciences. After the first proof of principle of microchip CE in the early 1990s [1–4], a variety of separation problems have been addressed in microfluidic systems [5–7] and realized in various materials, accessible – last but not least – through the advances in microtechnology and microfabrication.

Microfluidic devices can nowadays be fabricated with integrated sample pre-treatment and post-treatment components, such as mixers, concentrators, filters, etc. Many detection principles such as spectroscopic and electrochemical analyses as well as coupling to mass spectrometers have been demonstrated in microchip format. Microscale separations offer – in addition to low analyte and sample consumption, little waste and reduced costs – a gain in performance and analysis time as well as high-throughput capabilities by parallelization.

Correspondence: Dr. Alexandra Ros, Experimental Biophysics and Applied Nanosciences, Physics Department, Bielefeld University, Universitätsstrasse 25, D-33615 Bielefeld, Germany
E-mail: alexandra.ros@physik.uni-bielefeld.de
Fax: +49-521-1062959

Abbreviations: **AC**, alternating current; **ANM**, absolute negative mobility; **GFP**, green fluorescent protein; **OT**, optical tweezers; **Sf**, *Spodoptera frugiperda*; **YFP**, yellow fluorescent protein

The importance of microfluidic devices for bioanalysis has been explicitly underlined by the first commercial microchip devices such as the Bioanalyzer from Agilent or the Experion from BioRad.

Moreover, it became clear that microfluidic and nanofluidic components offer a much broader and more complex horizon than originally thought by scaling down macroscopic bioanalytical technologies. Upon entering this new domain of science, individual biomolecules can be detected and quantitatively analyzed and minute volumes can be handled that are smaller than that of an individual cell. In addition, nanofluidic environments can be produced that are on the length scale of molecules or their characteristic mean free paths allowing fascinating new concepts and phenomena for microseparation and nanoseparation.

For instance, the coupling to nanoscale fluidic channels allows to exploit electrokinetic effects at the double layer thickness, resulting in efficient preconcentrators [8] or the creation of pH gradients [9]. Furthermore, migration phenomena have been investigated on the basis of thermal fluctuations in combination with asymmetric periodic potentials usually referred to as molecular ratchets [10], which have also been applied to biomolecules [11–13]. Entropic trapping [14, 15] and tailored geometrically structured microdevices [16–18] represent examples of DNA separation devices for fragment sizes larger than 20 kbp – a size range which is rarely accessible by CE. Microfluidic devices also allow the handling and posi-

tioning of single cells [19] and chromosomes [20] as well as on-chip lysis and electrochemical [19, 21] as well as fluorescence detection [22, 23] opening promising perspectives for single cell analysis in systems nanobiology and proteomics [24]. All these developments have in common the use of structured microfluidic and nanofluidic components giving rise to novel manipulation tools and unexpected phenomena for microseparations and nanoseparations.

In this paper, we address three novel microfluidic developments for bioanalysis in tailored microfluidic systems realized in PDMS. In Section 3.1, we demonstrate a single cell analytical method for proteins which combines a structured microfluidic device with latest optical laser technology for single cell manipulation (trapping and steering), free-solution electrophoretic protein separation and protein detection. In particular, we focus on electrical on-chip lysis and single cell protein electropherograms with single and multiple transfections detected by visible LIF (VIS-LIF) detection.

In Section 3.2, we exploit dielectrophoresis for the separation of large genomic DNA fragments in microfluidic channels structured with periodic obstacle arrays. We demonstrate the successful dielectrophoretic trapping of large T2-DNA (164.5 kbp) by the application of an alternating current (AC)-electrical field and a first electropherogram for DNA separation.

In Section 3.3, we focus on a new migration phenomenon, utilizing thermal fluctuations in a nonequilibrium environment to generate a rather surprising and paradoxical migration behavior termed absolute negative mobility (ANM). Here, negative mobility is referred to the average motion of a Brownian particle in the direction opposite to an applied static force. This phenomenon has recently been demonstrated to occur for colloidal particles in structured microdevices [25] and we discuss its potential application for separations in microfluidic bioanalysis.

2 Materials and methods

2.1 Chemicals and reagents

PDMS (Sylgard 184) was purchased from Spoerle Electronic (Germany), glass microscope slides from Menzel (Germany). Pullulan, Tween 20 and EDTA were obtained from Sigma (Germany), POP-6 from Applied Biosystems (USA) and YOYO-1 from Molecular Probes (Germany). PBS tablets, CHES, Tris, T2-DNA, β -mercaptoethanol, sodium chloride and L-histidine were purchased from Fluka (Germany). The triblock copolymer Pluronic F-108

was a generous gift from BASF (Germany). SDS was from Merck (Germany). For all solutions deionised water from a Milli-Q biocel (Millipore, USA) was used. Carboxyl-modified fluorescently stained polystyrene particles (CML microbeads) of 1.9 μm diameter as well as CML beads of 2.8 μm diameter were obtained from Interfacial Dynamics (USA).

2.2 Cells

Sf9 insect cells (*Spodoptera frugiperda*) from Novagen (USA) transfected with pEX4-vector (Novagen) containing the genes for the fusion proteins were used in these studies. For single cell electropherograms with one transfection, Sf9 cells expressed a green fluorescent protein (GFP)-labelled 'loss-of-function' mutant of the cytoplasmatic G-protein ArF1 of *Medicago truncatula* (T31N-GFP, molecular mass 49.5 kDa). For single cell experiments with two transfections, the proteins Pep12-yellow fluorescent protein (YFP) (50 kDa) and γ -PKC-GFP (105 kDa) were expressed by the Sf9 cells. Portions of the cell culture (200 μL) in BacVector insect cell medium (Novagen) were washed with PBS buffer (10 mM phosphate, 137 mM NaCl, 2.7 mM KCl, titrated to the optimal cell medium pH of 6.4) via centrifugation and subsequent buffer addition. An estimated concentration of 10^5 cells/mL served for the single cell manipulation and lysis experiments.

2.3 Fabrication of PDMS devices

A master with the inverted relief of the microstructure was fabricated by spincoating a photoresist (SU-8) onto a Si-wafer, UV-exposing through a chromium mask and development in a developer bath. The detailed fabrication procedure was recently published [26]. Briefly, the polymer Sylgard 184 and its curing agent were mixed in a 10:1 ratio and poured over the microstructured wafer. After curing, the crosslinked polymer was easily peeled off the wafer and the reservoir holes were punched. Before assembly, PDMS slabs or a clean glass slide were oxidised in an in-house-built oxygen plasma chamber for 30 s. The microstructures were either sealed with a glass slide or a PDMS slab. The microfluidic channels were coated with the triblock copolymer F-108, significantly reducing adhesion of cells and colloidal particles, or a poly(oxyethylene)-silane for DNA migration experiments [27]. Exact chip dimensions for the single cell experiments and for the ANM experiments are given in [24] and [25], respectively. The dielectrophoretic microfluidic chips consisted of four channels, creating an injection cross at their intersection. Three channels were 2 mm long and had a cross section of $\sim 95 \times 6 \mu\text{m}^2$. The separation

channel was 5 mm long and had a cross section of $99 \times 6 \mu\text{m}^2$. The rectangular posts had a base of $7.4 \times 2.2 \mu\text{m}^2$ and were $6 \mu\text{m}$ high, equal to the channel height in the whole device. The rows of posts had a distance of $21 \mu\text{m}$ and the gap size between the posts was $2.3 \mu\text{m}$.

2.4 Cell steering and microfluidic handling

Individual Sf9 cells were trapped, injected and steered in the microfluidic channel by an in-house-built single-beam optical tweezers (OT) system which was incorporated into an inverted optical microscope [28] with additional standard fluorescence microscopy capabilities in the visible range. A selfconstructed x/y -stage allowed long-range positioning of cells with the OT within the microchannel for maximal 25 mm with a precision of $1\text{--}2 \mu\text{m}$. By this means, an individual cell can be trapped in the reservoir and navigated to the injection position. Cell movement and lysis was observed using a CCD camera (DMK 3002-IR/C, The Imaging Source, Germany) grabbing images at a rate of 25 frames *per* second. Electrical lysis was performed by applying $>3000 \text{ V}$ for pulse periods of $>50 \text{ ms}$ to the separation channel (total length 24 mm). SDS-lysis was performed by flushing buffer containing 1% SDS over the trapped cell, as described previously [24]. Details for the injection conditions and the used buffers are provided in the figure legends for the corresponding electropherograms.

2.5 Detection

Fluorescence detection of proteins during separation was performed on an inverted microscope using VIS-LIF detection, as previously described [24]. The detection point for VIS-LIF was adjusted for the individual experiments according to the chip dimensions, usually several millimetres. Particle motion for the negative mobility experiments was recorded on an inverted microscope using a $\times 20$ objective and a sensitive CCD-camera (Sensicam, LaVision, Germany). The velocity of the colloidal particles was analyzed by particle image velocimetry (PIV) using ImageJ freeware and Plugin MTrack2 (Nico Stuurman, University of California, San Francisco). DNA in separation buffer (10 mM phosphate, 2 mM NaCl, 1 mM EDTA, 0.2% β -mercaptoethanol *v/v* and 0.1% POP-6 *v/v*), fluorescently stained with the intercalator YOYO-1, was recorded with a sensitive CCD-camera according to [26].

2.6 Chip operations

Initial filling of the microchannels was performed either by capillary action or by the application of vacuum to the reservoirs. Electrical connection to the microchip device was achieved with platinum electrodes dipped into the reservoirs. Direct current (DC) and AC voltage for injection, trapping, lysis and separation were applied using power supplies from FUG (Model MCN 14-2000, HCN 14-12500 and HCN 7E-12500, Germany), a DAQ-card (6036E, National Instruments, USA) and an amplifier unit (600H, NanoTechTools, Switzerland). Instrumental control and data acquisition were performed by software programmed in LabView (National Instruments).

3 Results and discussion

3.1 Single cell analysis

The microfluidic single cell analysis method is depicted in Fig. 1. In order to avoid cumbersome single cell micro-mechanical manipulation, we have developed a method which completely uses on-chip operations for single cell selection [24]. For this purpose, a cell ensemble is suspended in one reservoir of the microfluidic device. In step 1, an individual cell of interest (*e.g.* a transfected cell) can be selected by optical inspection and subsequently trapped with OT. During step 2, this particular cell is navi-

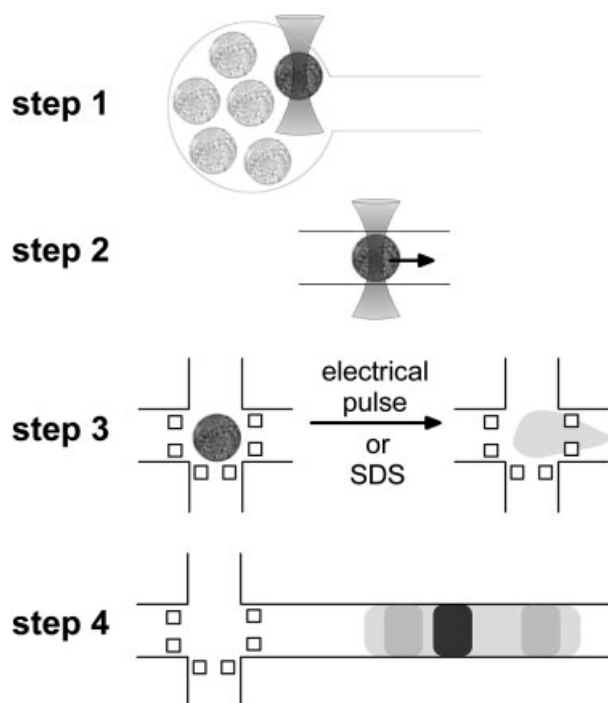


Figure 1. Steps 1–4 of the microfluidic single cell analysis method (for details see text).

gated along the microchannel to an intersection of two channels, which is structured by posts and acts as a physical trap. In step 3, the cell is lysed at the intersection position. Subsequent electrophoretic migration leads to the transport and separation of the protein components of the cell which are detected by VIS-LIF in the separation channel during step 4.

Figure 2 demonstrates experimental snapshots of steps 1 and 2 of our single cell analysis method. The transfection efficiency of one GFP-mutant in the used Sf9 insect cells was typically between 20 and 50%. This is strikingly demonstrated by the fluorescence microscopy images of a cell population in Figs. 2a and b. The inspection of the cell population provides information about the transfection efficiency and the status of the cells. By this method, we were able to preselect cells of interest by OT trapping, for example only fluorescently altered cells in a biologically vital state. Following navigation of the selected cell along the microchannel is demonstrated in Fig. 2c. Finally, the captured cell is trapped at the intersection position in Fig. 2d.

In a previous publication [24], we could show that Sf9 cells trapped at the intersection can be lysed by SDS-containing buffers within seconds. The lysis time deter-

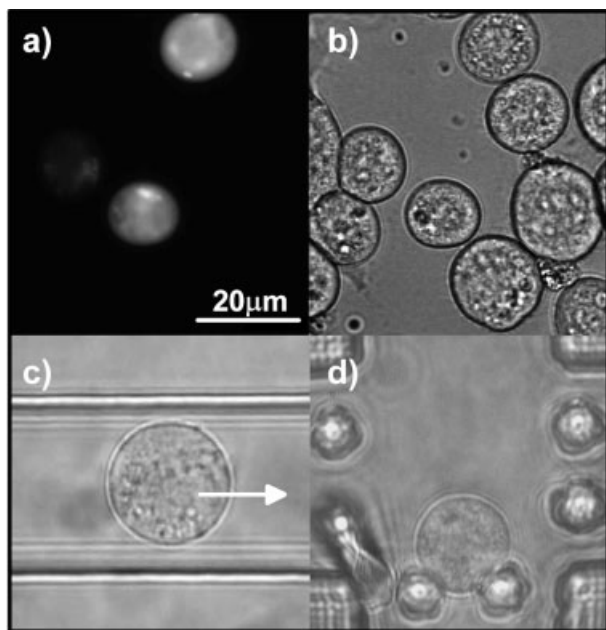


Figure 2. Ensemble of transfected Sf9 cells observed by fluorescence microscopy (a) and bright field microscopy (b). Clearly, transfections were not successful for the whole cell population. (c) An individual Sf9 cell is navigated with OT through a linear channel to the injection position, as indicated by the arrow. (d) A physically trapped Sf9 cell at the injection position. Post dimension: $8 \times 8 \mu\text{m}^2$; height, $\sim 30 \mu\text{m}$.

mines the injected plug length and is critical in terms of band broadening for subsequent protein separation. Thus, fast electrical lysis was recently adapted to our microchip format. The cells were subjected to high voltage pulses above $3000 V_{p-p}$ for several milliseconds ($>50 \text{ ms}$) inducing complete lysis. Figure 3 demonstrates a sequence of fluorescence images of the cell lysis process of a transfected Sf9 cell. Clearly, fluorescent cell components are injected towards the separation channel (on the right) within the 120 ms observation sequence. Figure 4a demonstrates a single cell electropherogram of a transfected Sf9 cell after electrical lysis. Explicitly, a single component peak is detected after electrical lysis at 1250 V/cm for 50 ms, confirming the detection of a single fluorescent protein component in the single cell electropherogram.

In additional experiments, individual co-transfected Sf9 cells exhibiting two fusion proteins, namely γ -PKC-GFP and Pep12-YFP, were tested in our microfluidic device.

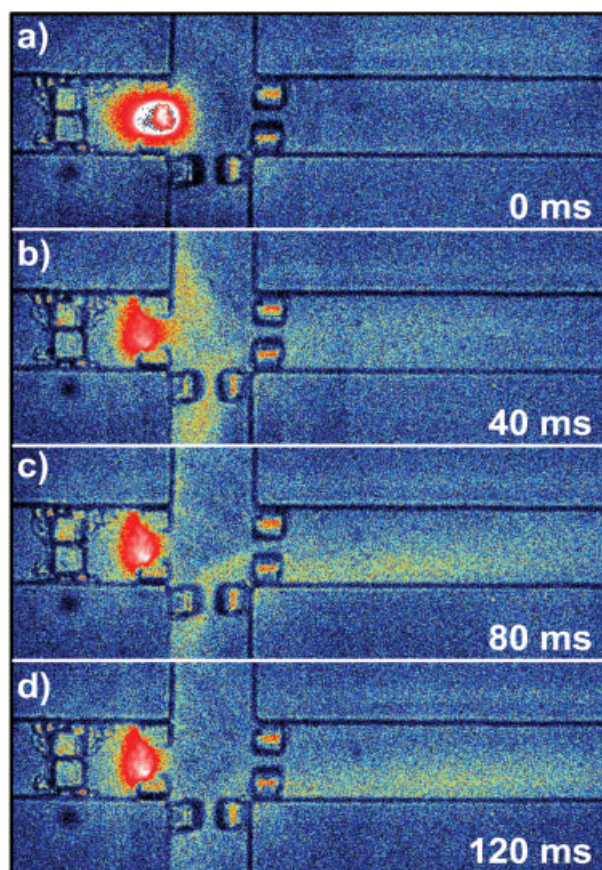


Figure 3. Sequence of fluorescence images (a–d) of the injection process of the content of a single Sf9 cell into the separation channel. After an electrical pulse (4000 V/cm at 100 ms), the content of the cell is electrokinetically transported towards the detector at a separation field strength of 420 V/cm in PBS buffer.

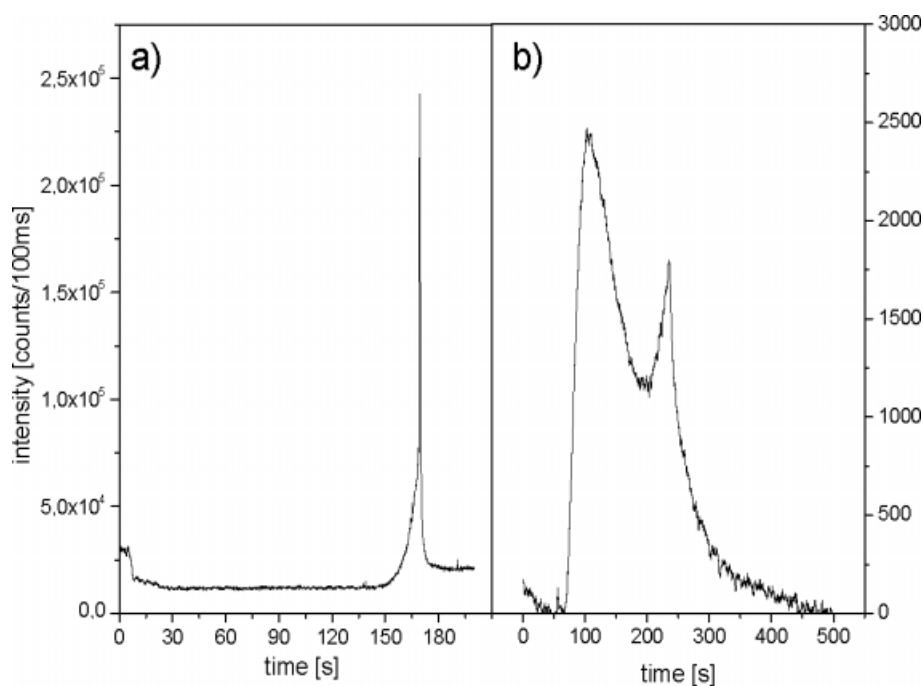


Figure 4. (a) Single cell electropherogram of an electrically lysed Sf9 cell expressing T31N-GFP with VIS-LIF detection. Detector was placed at a distance of 8 mm from the injection and lysis position. Electrically induced lysis was achieved by a pulse of 50 ms at 1250 V/cm, the following electropherogram was recorded at 830 V/cm (separation buffer: 4% Pullulan in 100 mM CHES/Tris). (b) Single cell electropherogram of an Sf9 cell expressing both Pep12-YFP and γ -PKC-GFP recorded at 15 mm separation distance (separation buffer: 4% Pullulan, 1% SDS, 0.1% POP-6 v/v, 100 mM CHES/Tris). Clearly, the electropherogram demonstrates two peaks for the two fluorescent proteins in the cell.

Although our VIS-LIF detector is capable of detecting both fluorescent proteins (GFP and YFP), a smaller fluorescence intensity is expected in our setup for YFP due to its emission maximum shifted to longer wavelengths and the used filters. Figure 4b demonstrates the obtained electropherogram after chemical lysis with SDS, which clearly exhibits two peaks stemming from the GFP- and YFP-mutants. It is worth noting that this electropherogram was obtained with considerably different parameters for lysis, injection and separation as well as in another separation buffer compared to the electropherogram with electrical lysis of a single cell with the fluorescent protein mutant T31N-GFP in Fig. 4a (see also Fig. 4 and Section 2) leading to reduced migration times and broader protein peaks.

Having demonstrated the proof of principle of our microfluidic approach for single cell trapping, lysis and separation analysis, we are interested in the potential application of this method for proteome research. We could recently show that dye molecules can be detected in concentrations as small as 100 fM with our VIS-LIF detector [16]. Calculating the protein concentrations in single cells confined in microenvironments, we can estimate the necessary detection sensitivity for single cell protein detection. Assuming a 10 μ m sized cell (comparable to an Sf9 cell) in a cube of volume 10³ μ m³ (~1 pL) a detection sensitivity of 100 nM is required for a low abundant protein present at a copy number of 10⁵ in a cell. Thus, the sensitivity of our detector complies with

calculated analytical needs to detect low-abundant proteins in single cells, which will be addressed in the near future.

3.2 Large genome DNA separation

For the separation of large genomic DNA, we have constructed a linear microchannel with a periodical array of posts, which allows electrodeless dielectrophoretic trapping of DNA upon application of an AC voltage, according to the method of Chou *et al.* [29]. The posts (2.2 \times 7.4 μ m²) are separated by an in-line distance of 2.3 μ m at an array distance of 21 μ m. The structured microchannel had a width of 99 μ m and was connected to a cross injector of similar channel dimensions. T2-DNA was subjected to an AC voltage and successfully trapped in the microdevice as recorded by fluorescence video microscopy (see inset of Fig. 5). It could be clearly demonstrated, that complete trapping of DNA in solution was achieved with a DNA-concentration of 9 pM. The trapping process was reversible for short trapping times, *i.e.* the periodic activation of the AC-voltage led to successful trapping of free diffusional DNA molecules.

In subsequent experiments, T2-DNA was injected by the pinched injection method *via* the cross injector and the DNA was subjected to migration within the microstructure array with an AC voltage superimposed by an additional offset voltage (see caption of Fig. 5 for details). The AC voltage was switched off at a distinct and preset time

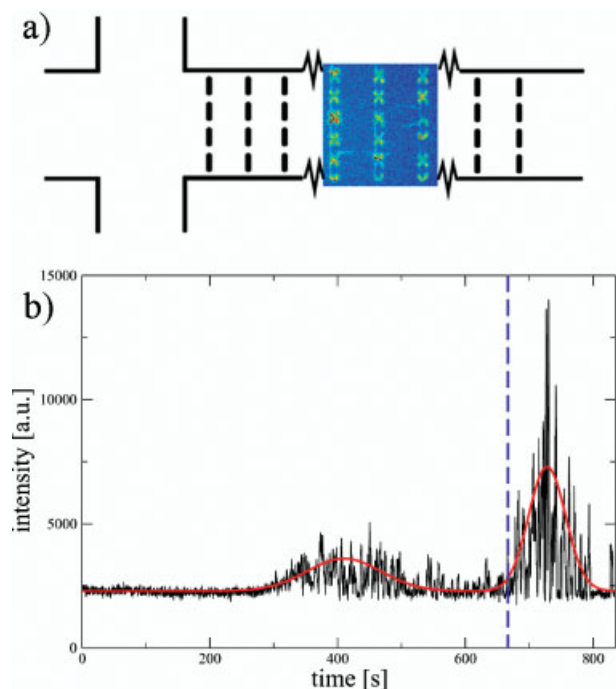


Figure 5. (a) Schematic drawing of the microfluidic layout for dielectrophoresis experiments demonstrating a cross injector connected to the structured separation channel. Electrodes were dipped in each reservoir for electrical connection (not depicted). All channels were 2 mm except the separation channel, which was 5 mm long. Dielectrophoretic traps are created by the electrical field gradient along the small gaps between the posts (thick vertical lines in the separation channel). Coloured inset represents a fluorescence microscopy image of a section of the structured separation channel in which fluorescently stained T2-DNA is dielectrophoretically trapped forming x-shapes. (b) Recorded electropherogram for T2-DNA in a structured microchannel subjected to dielectrophoresis. T2-DNA at a concentration of 9 pM was injected by pinched injection, the detector was placed at 3.8 mm. A sinusoidal AC voltage of 144 V at a frequency of 60 Hz with an additional offset of 12 V was applied for 667 s. During this period, only small DNA fragments passed the detector (first peak). After release of the dielectrophoretic force at 667 s (see dashed line), longer T2-DNA molecules passed the detector (second peak). Red line represents a Gaussian fit to the electropherogram as a guide to the eye.

during the migration experiment. The electropherogram as depicted in Fig. 5b was observed by recording the fluorescence signal at a position of 3.8 mm from the injector. Clearly, two peaks were recorded, where the first peak is attributed to DNA molecules, which were not dielectrophoretically trapped during application of the AC potential. Obviously, the trapping force was not sufficient to retain these molecules in the structured microdevice.

After deactivation of the dielectrophoretic force, a second DNA peak was recorded, indicating that DNA molecules have been trapped in the device and were released after switching off the AC potential. Careful inspection of the recorded video data could provide an explanation for this finding. T2-DNA molecules with a size of 164 kbp were released only after deactivation of the field, whereas smaller DNA fragments were detected during AC voltage application. Such small molecules can emanate from shear force fragmentation during sample handling or are impurities of the sample.

Chou *et al.* [29] gave first evidence that dielectrophoretic trapping of DNA in microstructure arrays is dependent on AC voltage and fragment size, and we propose here that it can be exploited for the separation of large genomic fragments in tailored microfluidic devices. We are currently extending these studies to advanced geometries and AC conditions, in order to enhance separation efficiency and, to determine the applicable DNA-size range and type for dielectrophoretic genomic DNA separation or purification.

Several advantages arise for future dielectrophoretic separations for DNA-molecules. First, adjustment of suitable trapping forces – easily tuned by the applied AC voltages – allows for complete trapping of a certain molecular size thus providing efficient separation or purification. Further, a DNA-fragment size range (>20 kbp) which is hardly addressed in capillary format becomes accessible, as previously demonstrated by other new methods based on molecular dynamics in microstructured devices [12, 13, 15, 16, 18] and the separation is very fast (<15 min) compared to time consuming PFGE in slab gel format.

3.3 Paradoxical migration

Thermal fluctuations in a nonequilibrium environment can be utilised to generate a rather surprising and paradoxical migration behavior termed ANM. ANM is referred to the average motion of a Brownian particle in the direction opposite to an applied static force. This phenomenon was originally predicted theoretically in simplified model systems [30] and recently experimentally realised in a structured microfluidic device with micrometer-sized colloidal particles [25].

More precisely, ANM can occur in a microdevice with periodically arranged posts, which alternately exhibited gaps (distance between obstacles bigger than the bead diameter) and traps (distance between obstacles smaller than the bead diameter) along the channel and perpendicular to the channel axis (see inset of Fig. 6). Applying an AC voltage U_0 with an additional (small) offset bias U_{DC} to

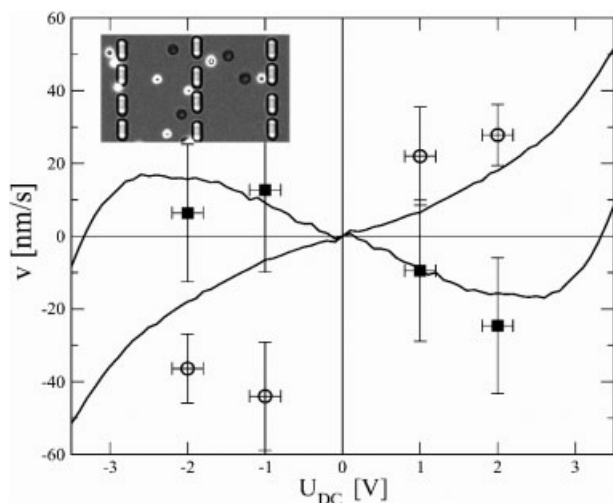


Figure 6. Velocity of latex beads as a function of applied static offset voltage U_{DC} . Beads were subjected to a periodical driving voltage $U_{AC} = 5$ V at a period of 140 s. Beads of diameter $1.9 \mu\text{m}$ (squares) show ANM whereas the beads of diameter $2.8 \mu\text{m}$ (circles) demonstrate 'normal' behaviour. For small U_{DC} , these beads can be steered into opposite directions (buffer conditions: 100 mM phosphate (pH 8.3), $200 \mu\text{M}$ Tween 20, and $100 \mu\text{M}$ L-histidine). Inset demonstrates a bright field microscopy image of a section of the structured microchannel filled with both fluorescent ($1.9 \mu\text{m}$, bright dots) and nonfluorescent ($2.8 \mu\text{m}$, dark dots) beads.

beads suspended in this tailored microfluidic device invokes particle migration in the direction opposite to the applied static force U_{DC} . This paradoxical nonequilibrium effect can only occur by a combination of Brownian motion (thermal noise), a periodic driving and nonlinear dynamics induced through the structuring in the microfluidic device. A detailed explanation of this mechanism is given in [25] and is beyond the scope of this paper.

Fundamentally based on Brownian motion and thermal nuisance, it is of particular interest to study the responses of differently sized particles under ANM conditions. We have thus subjected carboxylated latex particles of different diameters to a periodic driving voltage U_0 and recorded the corresponding particle velocities for different values of U_{DC} . For small values of U_{DC} , we could indeed verify the coexistence of negative mobility for small particles and 'normal' migration behaviour for larger particles. Figure 5 demonstrates the experimental data together with numerical simulations adapted to the experimental conditions (for a detailed description of the numerical simulations see [25]).

These results demonstrate explicitly that the phenomenon of negative mobility can be tailored to conditions where particles of different sizes can be directed into

opposite directions, controlled by the value of the static perturbation U_{DC} . Obviously, this size-dependent negative mobility may be exploited for separation or fractionation of micrometer-sized colloidal particles and also biological compounds of comparable size, like cells or cell organelles. Note that our experimental demonstration of negative mobility has been performed under biological buffer conditions, so that the effect is also expected to occur for biological macromolecules. Since theoretical predictions of negative mobility in structured geometries remain valid for point-like particles [30–32], we may even observe negative mobility in suitably designed nanostructures for biomolecules, such as DNA and proteins. This effect is then also expected to be sensitive to particle properties, e.g. the length of the DNA molecule, and thus may serve as an efficient and flexible separation technology for biomolecules, that could be easily integrated into 'lab-on-a-chip' devices.

4 Concluding remarks

Three examples of novel perspectives for microfluidic bioanalysis were demonstrated, which are all based on particularly structured microfluidic channel systems and extend common separation concepts by exploiting new phenomena for molecular dynamics on a length scale of $10 \mu\text{m}$ and below. They comprehend physical cell traps for single cell analysis on microfluidic platforms (Section 3.1), novel physical migration phenomena such as the exploitation of dielectrophoresis for DNA fragment separation or purification (Section 3.2) and ANM for the separation and fractionation of colloidal particles (Section 3.3). In the future, these novel developments will be extended to effective and rapid analysis and separation devices for biomolecules, cell fragments or cells. Single cell fingerprinting with on-chip protein detection in the visible range as well as with label-free UV LIF detection of proteins is also anticipated.

Sf9 cells were generously donated by Nickels Jensen and Professor Karsten Niehaus from the Department of Genetics from Bielefeld University. Andy Sischka, Dr. Katja Tönsing and Christoph Pelargus from the Experimental Biophysics Group at Bielefeld University are acknowledged for technical assistance. Special thanks are dedicated to Professor Peter Reimann and Dr. Ralf Eichhorn of the Condensed Matter Theory Group at Bielefeld University for numerous helpful discussions and the numerical simulations accompanying the ANM experiments. Financial support from the Deutsche Forschungsgemeinschaft within the project An 370/1-2 and the collaborative research project SFB-613 (project D2) is gratefully acknowledged.

5 References

- [1] Harrison, D. J., Manz, A., Fan, Z., Lüdi, H., Widmer, H. M., *Anal. Chem.* 1992, 62, 1926–1932.
- [2] Harrison, D. J., Fluir, K., Seiler, K., Fan, Z. et al., *Science* 1993, 261, 895–897.
- [3] Seiler, K., Harrison, D. J., Manz, A., *Anal. Chem.* 1993, 65, 1481–1488.
- [4] Effenhauser, C. S., Manz, A., Widmer, H. M., *Anal. Chem.* 1993, 65, 2637.
- [5] Auroux, P. A., Iossifidis, D., Reyes, D. R., Manz, A., *Anal. Chem.* 2002, 74, 2637–2652.
- [6] Reyes, D. R., Iossifidis, D., Auroux, P. A., Manz, A., *Anal. Chem.* 2002, 74, 2623–2636.
- [7] Vilkner, T., Janasek, D., Manz, A., *Anal. Chem.* 2004, 76, 3373–3386.
- [8] Foote, R. S., Khandurina, J., Jacobson, S. C., Ramsey, J. M., *Anal. Chem.* 2005, 77, 57–63.
- [9] Fa, K., Tulock, J. J., Sweedler, J. V., Bohn, P. W., *J. Am. Chem. Soc.* 2005, 127, 13928–13933.
- [10] Reimann, P., *Phys. Rep.* 2002, 361, 57–265.
- [11] Bader, J. S., Deem, M. W., Hammond, R. W., Henck, S. A. et al., *Appl. Phys. A* 2002, 75, 275–278.
- [12] Bader, J. S., Hammond, R. W., Henck, S. A., Deem, M. W. et al., *PNAS* 1999, 96, 13165–13169.
- [13] Huang, L., Cox, E., Austin, R. H., Sturm, J., *Anal. Chem.* 2003, 75, 6963–6967.
- [14] Han, J., Craighead, H. G., *Anal. Chem.* 2002, 74, 394–401.
- [15] Han, J., Craighead, H. G., *Science* 2000, 288, 1026–1029.
- [16] Ros, A., Hellmich, W., Duong, T., Anselmetti, D., *J. Biotech.* 2004, 122, 65–72.
- [17] Doyle, P. S., Bibette, J., Bancaud, A., Viovy, J.-L., *Science* 2002, 295, 2237.
- [18] Kaji, N., Tezuka, Y., Takamura, Y., Ueda, M. et al., *Anal. Chem.* 2004, 76, 15–22.
- [19] Gao, J., Yin, X. F., Fang, Z.-L., *Lab Chip* 2004, 4, 47–52.
- [20] Prinz, C., Tegenfeldt, J. O., Austin, R. H., Cox, E. C., Sturm, J. C., *Lab Chip* 2002, 2, 207.
- [21] Xia, F., Jin, W., Yin, X., Fang, Z.-L., *J. Chromatogr. A* 2005, 1063, 227–233.
- [22] McClain, M. A., Culbertson, C. T., Jacobson, S. C., Albritton, N. L. et al., *Anal. Chem.* 2003, 75, 5646–5655.
- [23] Munce, N. R., Li, J., Herman, P. R., Lilge, L., *Anal. Chem.* 2004, 76, 4983–4989.
- [24] Hellmich, W., Pelargus, C., Leffhalm, K., Ros, A., Anselmetti, D., *Electrophoresis* 2005, 26, 3689–3696.
- [25] Ros, A., Eichhorn, R., Regtmeier, J., Duong, T. et al., *Nature* 2005, 436, 928.
- [26] Duong, T., Kim, G., Ros, R., Streek, M. et al., *Microelectr. Eng.* 2003, 67–68, 905–912.
- [27] Hellmich, W., Regtmeier, J., Duong, T., Ros, R. et al., *Langmuir* 2005, 21, 7551–7557.
- [28] Sischka, A., Eckel, R., Toensing, K., Ros, R., Anselmetti, D., *Rev. Sci. Instrum.* 2003, 74, 4827–4831.
- [29] Chou, C.-F., Tegenfeldt, J. O., Bakajin, O., Chan, S. S. et al., *Biophys. J.* 2002, 83, 2170–2179.
- [30] Eichhorn, R., Reimann, P., Hänggi, P., *Phys. Rev. Lett.* 2002, 88, 190601.
- [31] Eichhorn, R., Reimann, P., Hänggi, P., *Phys. Rev. E* 2002, 66, 066132.
- [32] Cleuren, B., Van den Broeck, C., *Phys. Rev. E* 2003, 67, 055101.